

Article

An Experimental Study: Variation Law of Magnetic Field around Concrete during Loading

Liming Qiu^{1,2,3,4}, Yongjun Tong^{1,2}, Jie Li^{1,2}, Dazhao Song^{1,2,*}, Man Wang⁴  and Shan Yin^{1,2}

¹ State Key Laboratory of the Ministry of Education of China for High-Efficient Mining and Safety of Metal Mines, University of Science and Technology Beijing, Beijing 100083, China; qiulm@ustb.edu.cn (L.Q.); gansutyj@163.com (Y.T.); 17806245008@163.com (J.L.); ysviola@163.com (S.Y.)

² School of Civil and Resources Engineering, University of Science and Technology Beijing, Beijing 100083, China

³ State Key Laboratory Cultivation Base for Gas Geology and Gas Control, Henan Polytechnic University, Jiaozuo 454000, China

⁴ State Key Laboratory of Coking Coal Exploitation and Comprehensive Utilization, Pingdingshan 467099, China; wangman.w@gmail.com

* Correspondence: song.dz@163.com

Abstract: In order to reveal the magnetic field response law and mechanism of concrete under load, the variation law of magnetic field intensity (MFI) of concrete samples under uniaxial loading, graded loading and cyclic loading was tested, and the field application scenarios of magnetic field monitoring technology are proposed. The results showed that a magnetic field signal would be generated during the loading failure process of the concrete sample, which was accompanied by the whole loading process. In the uniaxial compression process, MFI showed a steady increase trend, but it would increase rapidly when the load drop occurred in the sample. The stronger the rupture, the more significant the change of MFI. MFI was not linearly proportional to the amount of change in the load drop. MFI around the concrete sample was positively correlated with the load. When the concrete was in the constant load stage, MFI around the concrete remained basically stable. When the main rupture of the concrete sample occurred, MFI reached a peak value, it did not keep at a high level all the time, but decreased rapidly. There are two mechanisms for the generation of the magnetic field in the process of concrete failure under load, namely the piezomagnetic effect and the friction effect, which correspond to the action of the load and the excitation of the fracture, respectively. The former causes the stable increase of MFI, and the effect is related to the influence of the content of the piezoelectric magnetic material in the material composition; the latter leads to a sudden increase of MFI, and the effect is related to the triboelectric effect of the micro-particles of the material. The research results are conducive to the accurate prediction of the concrete magnetic field monitoring, and help promote the development of mine dynamic disaster monitoring and early warning technology.

Keywords: magnetic field intensity; concrete fracture; electro-mechanical coupling; monitoring and early warning



Citation: Qiu, L.; Tong, Y.; Li, J.; Song, D.; Wang, M.; Yin, S. An Experimental Study: Variation Law of Magnetic Field around Concrete during Loading. *Minerals* **2022**, *12*, 399. <https://doi.org/10.3390/min12040399>

Academic Editor: Alexander Mikhailovich Kalinkin

Received: 10 February 2022

Accepted: 21 March 2022

Published: 24 March 2022

Publisher's Note: MDPI stays neutral with regard to jurisdictional claims in published maps and institutional affiliations.



Copyright: © 2022 by the authors. Licensee MDPI, Basel, Switzerland. This article is an open access article distributed under the terms and conditions of the Creative Commons Attribution (CC BY) license (<https://creativecommons.org/licenses/by/4.0/>).

1. Introduction

With the rapid growth of the world economy, people's demand for mineral resources is getting stronger, leading to a continuous increase of mining intensity and depth. As a result, mine dynamic disasters are occurring increasingly, and disaster monitoring and early warning are becoming more and more important [1–3]. In the basic research on mine dynamic disaster monitoring and early warning, due to the difficulty of on-site sampling to ensure good repeatability and the complexity of the sampling process, in the process of laboratory research, the basic experiments are often carried out by using concrete to simulate coal and rock samples. As one of the primary building materials,

concrete has played an essential role in social development and construction due to its advantages of high strength, wide applicability and durability [4]. With the continuous improvement of the urbanization levels, large-scale public infrastructure such as dams, bridges, roads, houses and underground structures continue to increase rapidly. Therefore, using concrete samples to conduct basic experimental research, the results obtained have broader application prospects [5].

During the service process of the concrete structure, it will be jointly affected by a series of factors such as external load, structural aging and environmental corrosion. In recent years, safety accidents caused by concrete failure under load have still occurred from time to time. For example, on 3 December 2012, a collapse accident occurred in the Sasako Tunnel of the Chuo Expressway in Yamanashi Prefecture, Japan, resulting in a total of nine deaths. On 24 June 2021, the roof of an apartment building collapsed in Miami, Florida, killing 98 people. Safety accidents caused by the instability of concrete structures have seriously affected the safe development of cities. Accurate damage status identification and risk prediction of concrete structures are the key technologies to prevent and control such disasters. In particular, monitoring and safety evaluation of the early failure process of concrete materials is an important measure to prevent concrete instability disasters, and it is indispensable to develop this technology [6,7].

At present, most of the stress monitoring inside the concrete structure is to monitor the stress situation by burying sensors in the concrete structure [8], but this point-based monitoring method has great limitations. The location layout is complicated, the monitoring range is limited, and it is easily interfered by the construction of the concrete pouring process. The damage of the embedded sensor line is difficult to deal with, and the monitoring accuracy is difficult to guarantee. Therefore, finding an accurate and non-destructive monitoring method has become an important development direction of concrete monitoring technology.

The commonly used method for evaluating the stability of concrete structures is the comprehensive evaluation method based on constant weight, which obtains the comprehensive stability of concrete structures by calculating the stability and weight of each component [9]. This method has been widely used because of its simple principle and clear concept. However, the evaluation process of this method is not in real time; it belongs to the category of static evaluation method, and the value of weight is greatly affected by human factors. The comprehensive evaluation method based on variable weight, the analytic hierarchy process and the fuzzy evaluation method developed on this basis all have such shortcomings. It is challenging to realize the real-time monitoring and evaluation of the instability process of concrete structures. Major safety accidents in recent years have brought irreparable losses to human life safety, exposing the inadequacies of static assessment methods for concrete structure safety. In addition, the damage state of the concrete structure can also be evaluated by the method of sampling inspection and drilling peeping [10], but this technology belongs to the destructive inspection, which is not conducive to the stability of the concrete structure. At the same time, it still belongs to the category of static inspection and cannot achieve continuous testing.

At present, electro-geophysical monitoring technologies and methods are widely used in engineering structure instability monitoring and early warning. Due to the advantages of non-damage and continuous real-time monitoring, they have received extensive attention in this field. For example, Ji et al. [11] studied the size, age and loading method of concrete specimens, and the main factors affecting the acoustic emission (AE) characteristics of concrete were proposed. Wu et al. [12] studied the existence of the Kaiser effect and the existing stress range of concrete under the condition of reciprocating cyclic tensile loading. Wang et al. [13] studied the change characteristics of the wave velocity field during the concrete loading process, and found that the stress and time significantly affect the damage of the sample during the graded loading process. Using the "stress-time damage cumulative effect ratio" of AE, an early warning of concrete instability is proposed. Zhang et al. [14] analyzed the characteristics of magnetic property change in the rock failure process, and

found an obvious transition point shown by magnetic between any two adjacent failure stages. Zhang. [15] studied the AE characteristics of concrete with different aggregate contents, which provided a basis for monitoring concrete damage. Triantis et al. [16] studied the hidden affinities between electric and acoustic activities in brittle materials at near-fracture load levels, and found that the pre-failure indicators of the electric signals precede the respective ones of the acoustic signals.

The above monitoring methods for the internal damage of concrete mainly focus on wave monitoring, and have achieved certain results. However, the wave signal is often sudden during the concrete loading process, which is not conducive to the stable testing and quantitative interpretation of concrete structural damage. In contrast, the magnetic field monitoring method with better stability is less researched and applied in monitoring concrete damage, and the magnetic field monitoring method still has a relatively broad development space. Previous scholars have carried out theoretical and field studies on the stress, strain and magnetic field intensity (MFI) of brittle materials such as rock and concrete under compression. Chen et al. [17] implanted small magnets containing Nd-Fe-B in cylindrical marble and limestone and obtained the stress–strain–magnetic induction curve of the whole compression process through compression test. It is proved that the change of rock fissure can cause the change of magnetic induction, and a fitting relationship between stress and magnetic induction of rock is established. Zhang et al. [18] buried small Nd-Fe-B magnets in concrete containing magnetite powder, and the three-variable test of stress, strain and magnetic field in the process of monotonic loading, cyclic loading and unloading confirmed that there is a one-to-one numerical relationship concerning the stress–strain–magnetic field. It is proposed that the magnetic core can be pre-buried in large-scale structural components for online monitoring and prediction of its cracking and collapse. Previous studies have successfully demonstrated that fracture damage inside rock-like materials can lead to changes in MFI. This has played a pioneering role in the magnetic field evaluation technology to explore the internal damage of concrete structures. However, up to now, the research on the generation mechanism of the magnetic field effect in the concrete loading process is still insufficient, and the coupling relationship between the magnetic field and the concrete stress state is still unclear [19], which is not conducive to the development and application of this technology.

When the concrete is compressed and fractured, a magnetic field will be excited, which will cause the change of the electromagnetic field around the sample. Studying the relationship between load and the magnetic field is convenient for analyzing the damage of the concrete to achieve the purpose of using the magnetic field to monitor the internal damage of the material. Therefore, this paper intends to conduct concrete loading experiments to study the variation law of load, strain and magnetic field signal of concrete samples during loading, and explore the generation mechanism of the magnetic field effect on concrete under loading based on the test results. The research results will help to realize the accurate prediction of concrete magnetic field monitoring, and help to promote the development of monitoring and early warning technology for mine dynamic disasters.

2. Experimental Program

2.1. Sample Preparation

The cement used in this experiment is Taihangshan brand P.O42.5R ordinary Portland cement. The fine aggregate is river sand with a 0.5–2 mm particle size. After screening, the medium sand is used as the fine aggregate, and its various physical indicators are shown in Table 1.

Table 1. Physical index of fine aggregate.

Index	Apparent Density/kg·m ⁻³	Bulk Density/kg·m ⁻³	Mud Content/%	Fineness Modulus
Value	2950	1374	1.35	2.6

First, a cylindrical mold with a size of $\phi 50 \text{ mm} \times 100 \text{ mm}$ was used to prepare concrete samples. Cement, sand and water were added into the concrete mixer according to the set proportion and order for stirring. Second, the well-stirred slurry was poured into the concrete mold, and the mold was shaken through a vibrating table. After the treatment, the mold was placed in a $25 \text{ }^\circ\text{C}$ environment for two hours and then demolded. Lastly, according to national standards, the formed samples were placed in a YH-40B standard constant temperature and humidity curing box for 28 days. After curing, ends of the sample were ground to ensure that the flatness error of each end surface after grinding is less than 0.02 mm.

2.2. Experiment System

Previous studies have shown that coal, rock and concrete materials will release the energy accumulated inside them in the form of electromagnetic energy, sound energy, etc. [20], in the process of load failure. The research shows that the change of the magnetic field generated by the concrete is closely related to the load change. In order to further explore the change law of the magnetic field during the concrete failure process, a synchronous acquisition system (Figure 1) composed of loading control system, data acquisition system and electromagnetic shielding system was set up for signal monitoring of load, acoustic and magnetic. Through the time series analysis of load, magnetic field and AE signal, the characteristics of magnetic field change and its generation mechanism during uniaxial compression, graded loading and cyclic loading of concrete are quantitatively studied.

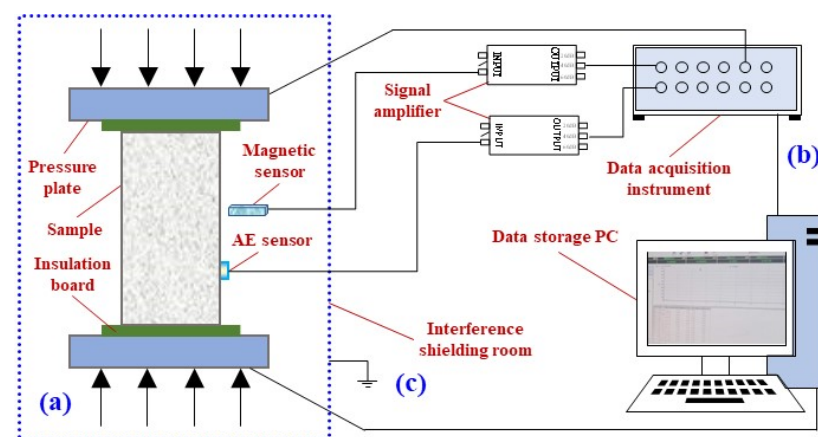


Figure 1. Experimental system diagram. (a) Loading system; (b) Data acquisition system; (c) Electromagnetic shielding system.

(a) Loading control system

The YAW-600 microcomputer (Jilin guanteng Automation Technology Co., Ltd., Changchun, China)-controlled electro-hydraulic servo pressure testing machine comprises the main engine, servo oil source, oil cooler, computer system and other parts. It is used to realize force closed-loop servo control and equal load loading in this experiment. The pressure testing machine has two control modes: Force control and displacement control, which can achieve high precision and constant load for a long time. The instrument can measure parameters such as compressive strength, and has been widely used to test compressive properties of various materials. The displacement resolution of the pressure testing machine is 3 N, the load resolution is 0.3 μm , the grating scale resolution is 0.1 μm , the extensometer resolution is 0.03 μm , the host stiffness is $> 5000 \text{ kN/mm}$, the controller sampling frequency is 1000 Hz and the maximum test force is 600 kN. The pressure testing machine cooperates with the corresponding computer software to realize the functions of real-time display of the experimental state, automatic collection and storage of test data and the functions of drawing various test curves simultaneously.

(b) Data acquisition system

The data acquisition system consists of a multi-channel magnetic field data collector and a data storage and analysis computer. The multi-channel magnetic field data collector has 10 three-axis fluxgate sensors to collect data simultaneously, can use the host computer software to read the collected data graph in real time and can realize the storage and playback of data. The sampling rate can be set to 100 Hz, 1 kHz, 10 kHz three gears.

The experimental setup is shown in Figure 2, the magnetic field sensor is located 5 cm around the sample for non-contact test, and the AE sensor is coupled with the sample surface with Vaseline. The magnetic field sensor is a Bartington-Mag-13MS100 (Bartington Instruments Co., Ltd., Oxford, UK) high-performance fluxgate sensor (Figure 3). The sensor range is $\pm 100 \mu\text{T}$, the resolution is 0.1 nT, the sampling frequency range is 0–3 kHz, the input signal voltage range is $\pm 10 \text{ V}$ and the quadrature error is less than 0.1° . AE monitoring adopts the Soft Island DS5 series 8-channel acquisition system, which consists of a data acquisition system, AE sensor and preamplifier. The maximum sampling frequency of the signal acquisition instrument is 10 MHz, the input signal voltage range is $\pm 10 \text{ V}$, and it can simultaneously record the full waveform data of all channels. The preamplifier input impedance of the AE sensor is greater than $10 \text{ M}\Omega$, the response frequency range is 50–400 kHz and the output impedance is 50Ω .

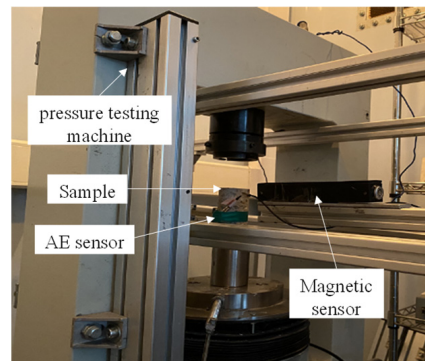


Figure 2. Experimental setup photo.



Figure 3. Magnetic field information collector.

(c) Electromagnetic shielding system

In order to shield the magnetic field changes caused by various items of external electrical equipment during the experiment, all experiments in this paper are carried out in the electromagnetic shielding room, to ensure the accuracy of the data during the experiment. Shielded indoor lighting is decorated in accordance with standard equipment rooms, and powered by high-performance low-leakage power filters. The shielding properties are as follows: 14 kHz $\geq 75 \text{ dB}$, 100 kHz $\geq 95 \text{ dB}$, 200 kHz $\geq 100 \text{ dB}$, 50–103 MHz $\geq 110 \text{ dB}$, 1–10 GHz $\geq 100 \text{ dB}$, 10–18 GHz $\geq 80 \text{ dB}$. In order to ensure the reliability of magnetic field test results, the whole experiment was carried out in the shielded room. The magnetic field

generated by the loading failure of the concrete sample was the difference between the actual tested strength value and the ambient MFI.

3. Analysis of Concrete Failure Form

After the experiment, the concrete was photographed, and the surface crack morphology of the concrete sample was obtained, as shown in Figure 4, where I, II represent the photographs at different shooting positions.

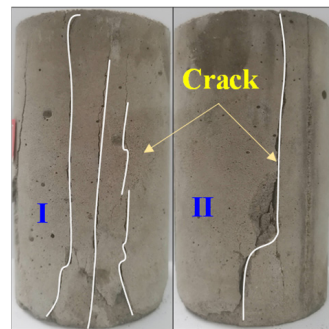


Figure 4. Crack morphology of concrete specimen.

The typical characteristics of cracks in the concrete specimen after failure are shown in Figure 4. There were three shallow cracks parallel to the loading direction on the I surface of the sample. There was an obvious shear failure mode on the II surface of the sample, and there was a crack running through the sample. In conclusion, the concrete exhibited obvious brittleness during loading, and there are many local fractures.

The concrete time-load curve was shown in Figure 5. It could be seen that the concrete sample roughly went through the compaction stage (O~A), the linear elastic deformation stage (A~B), the crack propagation stage (B~C) and the failure stage (C~D) during the uniaxial compression failure process.

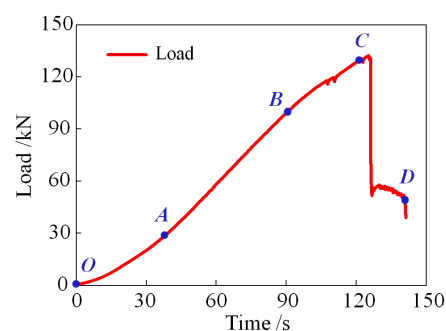


Figure 5. Typical loading curve of concrete specimen.

In the compaction stage (O~A), under the action of longitudinal load, the primary cracks inside the concrete sample gradually closed, and the load on the concrete gradually increased. In Figure 5, no load-drop occurred in the concrete specimen during the OA stage, indicating no significant failure and crack propagation at this stage.

In the linear elastic deformation stage (A~B), the overall mechanical curve showed an increasing linear trend. The force curve of the concrete specimen was basically linear, which indicated that the deformation of the concrete was uniform and its bearing capacity did not change. At this time, for the concrete sample, the state change was only load, and there was basically no damage, which was different from some heterogeneous rocks or coal.

In the crack propagation stage (B~C), new cracks were formed and expanded inside the sample, and penetrated through the original cracks, forming a crack network inside the concrete. Each failure would show a load-drop on the mechanical curve at this stage.

The load-drop in the BC segment in Figure 5 was not large, which indicated that the local failure inside the specimen was not violent. At this stage, the state change of concrete was not only load, but also damage, and the damage was accumulated continuously.

In the failure stage (C~D), the specimen fails and the load decreased rapidly. It is worth noting that, at the beginning of failure, the load near point C decreased very fast, and the bearing capacity dropped sharply. After a period of slow failure process, it suddenly failed again after point D. The phenomenon of multiple load-drops of the sample showed that the failure stage of the sample was composed of multiple failures, which was consistent with the shape of the crack in Figure 4.

4. Variation Characteristics of the Magnetic Field during Uniaxial Compression Failure of Concrete

Figure 6 showed the change law of the magnetic field in the failure process of concrete uniaxial compression. There were also significant differences in the characteristics of the magnetic field change in different load stages.

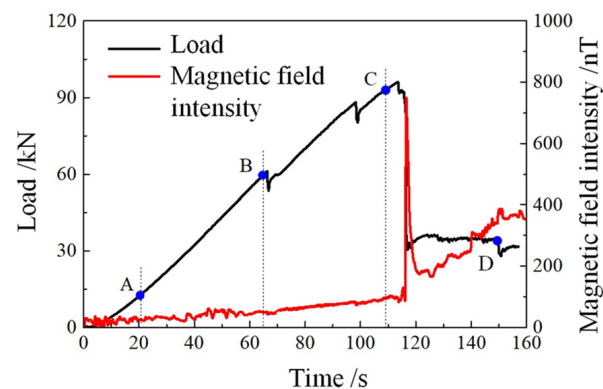


Figure 6. MFI curve of concrete sample.

In the compaction stage (O~A), when the concrete was in the compaction stage, the primary cracks inside the concrete sample were gradually closed under the action of longitudinal load, and the signal fluctuated at a low level. At this time, the fluctuation of the magnetic field might be related to the change of load and the closing of the crack, but due to the low load level and the small change of the crack, the fluctuation of the magnetic field was not large.

In the elastic deformation stage (A~B), since the original pores and cracks of the concrete had been closed in the compaction stage, when the load increased linearly with time, the internal elastic energy of the sample gradually increased. The steady increase of MFI around the sample might be related to load.

In the crack propagation stage (B~C), with the continuous expansion of the new crack, MFI around the sample fluctuated continuously. At this stage, the concrete load drop corresponded to the buckling failure inside the specimen, and MFI changed with the load. The local failure of the sample led to a decrease in the bearing capacity, the load of the sample decreased, and the internal energy of the concrete sample was released, resulting in an increase in the strength of the magnetic field around the sample. However, due to the relatively small scale of local damage at this stage, the increase of MFI was not large, and MFI mainly increased with the increase of load.

In the failure stage (C~D), with the continuous increase of the load on the concrete sample soil, when the load continued to increase to exceed the compressive strength of the sample, the sample was destroyed, MFI rose rapidly, and the concrete was completely unstable. After the destruction, MFI gradually stabilized. It is worth noting that, after the main rupture of the concrete specimen, the magnetic field did not maintain a high value, but decreased rapidly; after that, it rose to a certain height under the support of residual strength and stabilized. This phenomenon showed that both fracture and load could lead

to changes in the load of concrete samples, but the change of MFI caused by fracture was instantaneous, and the change caused by load was sustainable.

5. Characteristics of Magnetic Field Variation in Concrete Grading Loading Process

A force of 0.5 kN/s was controlled during the concrete grading loading process. When the pressure of the press on the sample is increased to 30 kN, 60 kN and 90 kN, the load was kept unchanged, and the constant load was 5 min. The peak loads received were 131.68 kN and 125.52 kN, respectively. The MFI test of the graded loading experiment used two fluxgate sensors, which were placed in the front and rear directions of the concrete sample, to more accurately record the relationship between the load and MFI.

The peak load of concrete graded loading was higher than that of concrete uniaxial compression failure. According to the research of Li et al. [21], the peak load of concrete showed a downward trend with the increase of loading rate, which was consistent with the results observed in this experiment.

Figure 7 showed the typical magnetic field change curve during the concrete grading loading process. The magnetic field strength of sample g1 (Figure 7a) and sample g2 (Figure 7b) has a good correlation with the load. Take sample g2 (Figure 7b) as an example, in the loading stage from 0~60 s, a large number of primary cracks in the concrete were closed, and MFI around the concrete was linearly related to the load. In the constant load stage from 60~360 s, the concrete was subjected to a constant load of 30 kN, and the magnetic induction intensity around the concrete was basically stable, and compared with the initial magnetic field, the magnetic field increased by 150~200 nT. In the loading stage 360~420 s, the load on the concrete increased to 60 kN at a constant speed, and MFI around the concrete also increased linearly with the load. In the constant load stage 420~720 s, the concrete was subjected to a constant load of 60 kN, and the surrounding area of the concrete was subjected to a constant load of 60 kN. The magnetic induction intensity remained basically stable, and increased by 250~350 nT compared with the initial MFI; in the loading stage 720~780 s, the load on the concrete increased to 90 kN, and the magnetic induction intensity of the concrete was linearly related to the load; in the constant load stage 780~1080 s, with the concrete at a constant load of 90 kN, the magnetic induction around the concrete was basically stable, rising by 350~450 nT compared with the initial magnetic field; the loading stage was 1080 s to failure, the concrete was gradually loaded to failure and the peak load before failure was 131.68 kN.

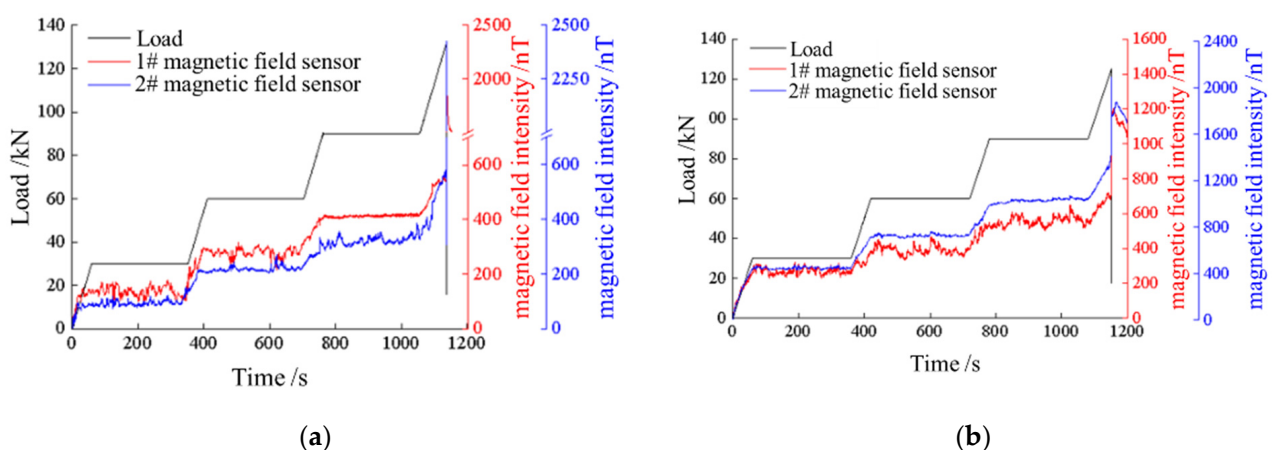


Figure 7. Load-magnetic curve of concrete during grading loading.(a) Sample g1, (b) Sample g2.

To sum up, in the process of concrete grading loading, MFI around the concrete sample was positively correlated with the load. When the concrete was in the constant load stage, the magnetic induction around the concrete remained basically stable, and with the increase of the dead load, the magnetic induction around the concrete also increased.

It is worth noting that, in the constant load stages, MFI presented a stabilizing tendency, but with relatively intense fluctuations. It showed that even when the load remains unchanged, small cracks in the sample were constantly generated, and these small cracks were random. Therefore, when the load was stable, MFI was still fluctuating.

Figure 8 showed the load-magnetic curve of the very last loading stage during grading loading of Figure 7b. We could see that when the macroscopic fracture was imminent, MFI increased rapidly and then decreased gradually.

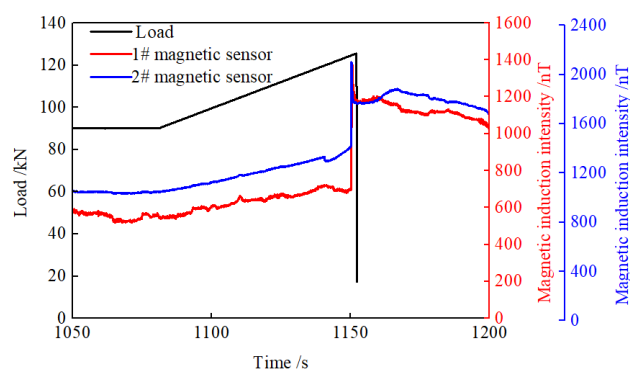


Figure 8. The load-magnetic curve of the last stage during grading loading.

6. Magnetic Field Characteristics of Cyclic Loading and Unloading of Concrete

Figure 9 showed the response curve of the magnetic field during the cyclic loading of concrete. The loading mode is displacement control. The magnetic field strength of sample c1 (Figure 9a) and sample c2 (Figure 9b) has a good correlation with the load. Take sample c1 (Figure 9a) as an example, it could be seen that during the cyclic loading and unloading process, MFI was positively correlated with the load. While there was no obvious load drop during the first cycle, MFI around the concrete still fluctuated during the rising process, while the falling process was relatively smooth. The reason for this might be that there were micro-cracks in the concrete during the load increasing process, which induced fluctuations of MFI, while no new cracks were generated during the load decreasing process. Therefore, the change of MFI was mainly affected by the load. During the second cycle, the change of MFI was similar to that of the first cycle loading process, and the fluctuation was still larger during the loading process, but smaller during the unloading process, which verified the above conjecture. During the third loading and unloading cycle, the changing law of MFI was similar to the first two cycles. During these three cycles, with the increase of the load peak value, the value of MFI also increased gradually, but the ratio of the increase of the two was not consistent, and the ratio of the increase of MFI was smaller than that of the load.

In the fourth loading process, the concrete sample suffered instability failure, and its magnetic field response characteristics were also different from those in the previous loading process, but MFI still increased gradually before instability occurred. With the appearance of the rupture, the change of MFI became severe; the greater the load drop, the greater the increase of MFI. When the main failure of the sample occurred, the magnetic field induction strength reached a peak value of 850 nT, and the signal strength far exceeded the first few cycle stages. These phenomena again verified that MFI was closely related to the rupture.

For Figure 9b, during the first two loading and unloading cycles, MFI was positively correlated with the change of load, and there was still a tiny fluctuation in MFI during the loading process, which indicated that the above phenomenon was repeatable. At the same time, the sample results in Figure 9 also showed that the change of MFI caused by the fracture was transient, and after the fracture, MFI would decrease to a relatively lower level.

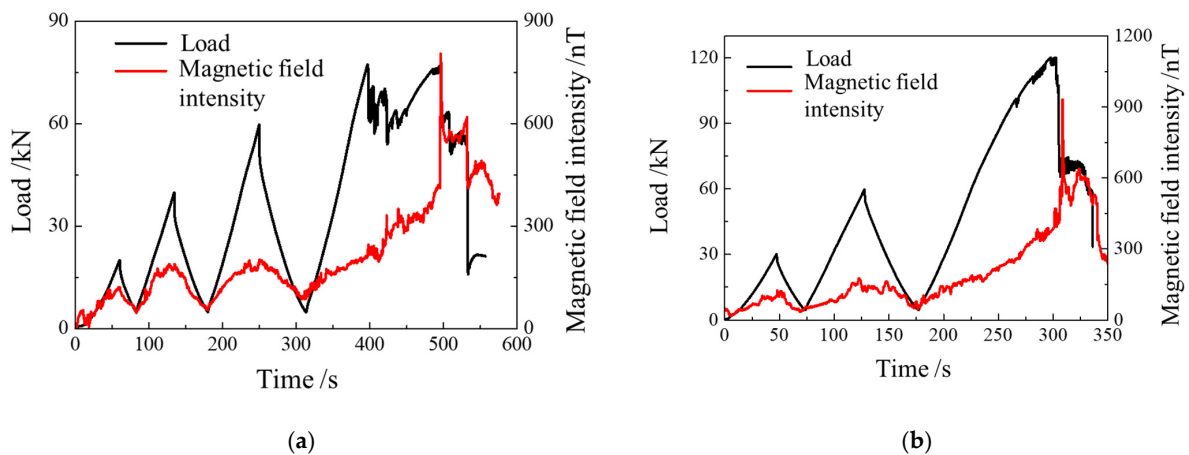


Figure 9. Variation law of the magnetic field of cyclic loading and unloading of concrete samples. (a) Sample c1, (b) Sample c2.

7. Discussion

7.1. Analysis of Damage and Failure Process of Concrete

AE is an effective means of monitoring the damage and failure process of concrete materials, reflecting the deformation and failure process of concrete. Combined with the AE monitoring method, the feasibility of the magnetic field monitoring method can be effectively verified. As shown in Figure 10, the AE signal parameters include energy, Ring Down Count (RDC), amplitude and so on. When the threshold value is set, the number of times the AE signal exceeds the threshold is RDC. Taking 1 s as the statistical period, RDC of AE can reflect the severity of sample failure. In this section, the comparative analysis of RDC and MFI was used to verify the relationship between concrete MFI and damage. During the test, the threshold was set to 45 dB.

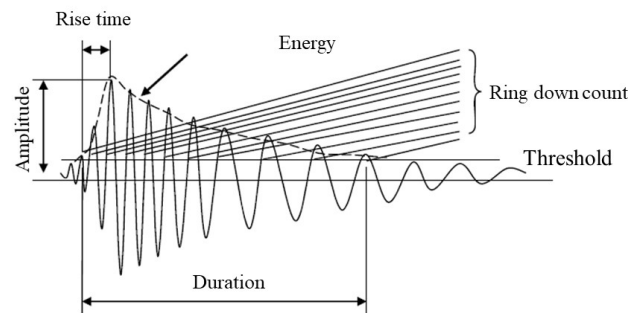


Figure 10. Schematic diagram of AE parameter definition.

It could be seen from Figure 11 that RDC of AE had a good consistency with the fracture. Before 50 s, there were hardly any ruptures in the concrete. Therefore, the AE signal was very minimal or even no signal. After 50 s, the sample began to continuously generate AE signals, indicating that the cracks inside the concrete were also continuously generated. Every time a large load-drop occurred, it was accompanied by a large RDC signal, and RDC reached its peak when the main rupture occurred. After that, the AE signal was still relatively dense, but the value of RDC was generally not high. Therefore, it could be considered that the fracture mainly occurred after 50 s in Figure 6; the two load-drops in the B~C section of the load curve both corresponded to relative fractures; the largest fracture occurred when the specimen was unstable.

Since acoustic emission could characterize concrete fracture, it could be used to verify the change law of the magnetic field when there was no fracture. Acoustic emission signal was minimal in the early load stage; the upward trend of MFI is obvious in Figure 11, which indicates that the increase of MFI was not completely caused by rupture.

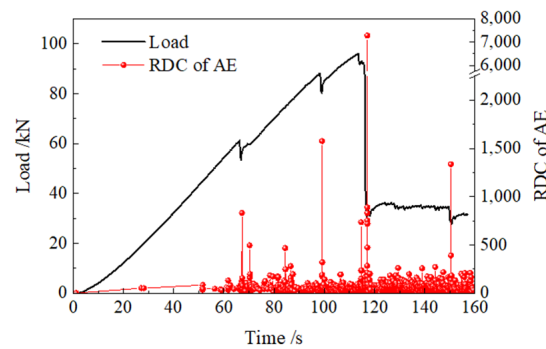


Figure 11. RDC of AE during loading of concrete samples.

Therefore, during the first 50 s loading process of the concrete sample, the load was the reason for the increase of MFI of the sample; in the subsequent process, the change of MFI was affected by the two factors of cracking and load. It seemed that the increase in load during the generation of small cracks could lead to a larger increase of MFI than in the case of no cracks. The rupture could also affect MFI, but its effect was greatly affected by the rupture strength. The stronger the rupture, the more significant the change of MFI. The variation of MFI was not linearly proportional to the variation of the load drop.

Similar findings were found in the study of Yin et al., shown in Figure 12 [22]. They found that at the moment of sample instability, the load curve could be observed to show a large fluctuation, the AE energy reached the maximum value and the corresponding magnetic induction intensity increased rapidly. Compared with the AE signals in the process of sample failure, they found that the change of magnetic field had good consistency with the deformation and failure of the sample. They did not carry out cyclic loading experiments and lacked further verification of the correlation between load and MFI. Under field conditions, the load changes of materials were complex, including loading, unloading and load retention. Therefore, a single loading method could not fully verify the feasibility of using magnetic fields to monitor the failure process of engineering structures under load. Different loading methods were used to carry out research, and the conclusions had wider applicability.

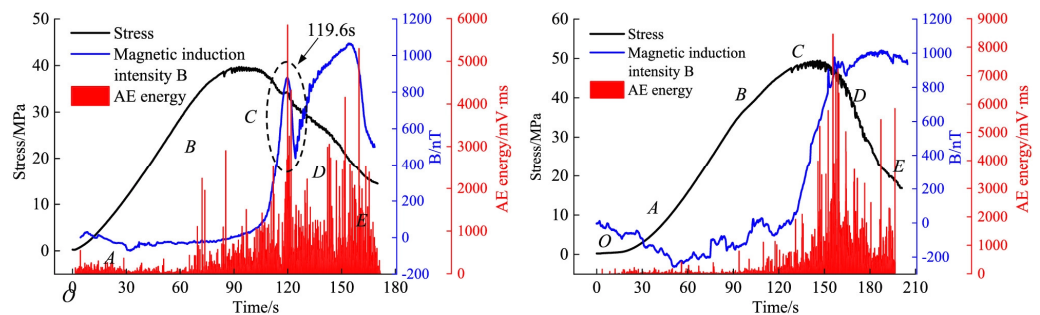


Figure 12. Results of Yin et al.'s research [22].

7.2. Analysis of Magnetic Field Response Mechanism in Concrete Loading Failure Process

Predecessors had extensively studied the failure modes of concrete, and it is currently believed that the failure process of concrete under uniaxial compression is essentially controlled by the tensile damage perpendicular to the direction of pressure action [23]. The factors that affect the failure form of concrete are: (1) The damage and failure of concrete originate from the fissures and cracks that exist before the concrete is loaded. The failure of concrete materials mainly comes from the expansion and penetration of microcracks caused by local tensile strain. (2) Concrete will deteriorate under the action of external load, and the deterioration position starts from the aggregate bond. (3) After the concrete is subjected to longitudinal compressive load, transverse tensile stress and tensile strain will

be generated inside, and when the tensile strain reaches the limit, the concrete material will be damaged.

There are two reasons for the geophysical effects of brittle materials caused by the loading failure process, one is the piezomagnetic effect, the other is the concrete failure process [24].

According to the piezomagnetic effect, under the action of an external force, the magnetic material will have an internal strain, which will cause its magnetic properties to change. The generation of the piezoelectric effect and magnetic domain structure in ferromagnetic materials are closely related to the change of the stress state. Magnetic domain refers to the small, disorganized area distributed in a ferromagnetic material, which is a basic feature of a ferromagnetic material. Before there is no load, the internal magnetic domains are disorganized and have no fixed direction for concrete materials. Since concrete is a brittle material, strain energy will be generated under the action of load, which will lead to changes in the internal magnetic domain structure of the concrete, thus being magnetized. The effect of magnetization is greatly affected by the composition of the concrete material. If the concrete contains piezomagnetic substances, the piezomagnetic effect is significantly better than that of the sample without compressive magnetic material. Figure 13 showed the loading failure process of the concrete sample containing magnets. Before 120 s, although there was no more significant damage, the change of MFI was still large, and the increase of MFI was much larger than that in Figure 6. Chen et al. [17] Implanted Nd-Fe-B magnetic core into rock samples and tested the variation law of MFI during rock loading and failure, as shown in Figure 14 [17]. They found that the variation law of stress–strain curve and MFI–strain curve was antisymmetric in the stage of rock fracture. Cyclic loading experiments did not occur in their work, either, and there was no load drop phenomenon on the loading curve, so it was difficult to judge the response of the instantaneous MFI of the fracture.

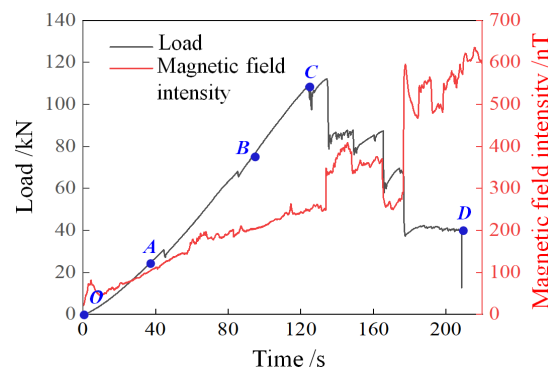


Figure 13. Variation curve of MFI of concrete containing magnets under loading failure.

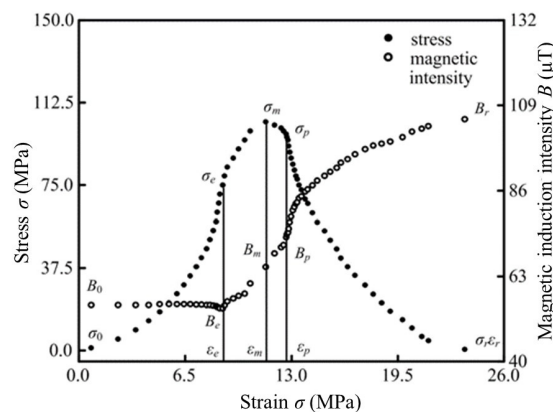


Figure 14. Results of Chen et al.’s research [17].

Under the action of uniaxial stress, the relationship between rock magnetic susceptibility K and stress σ is as follows [25],

$$K = K_0 \left[1 \pm \frac{\beta\sigma}{4} (3 \cos 2\theta + 1) \right] \quad (1)$$

where K_0 is the magnetic susceptibility when not loaded; θ is the angle between stress and magnetization direction; β is the proportion coefficient, which is generally 10^{-4} for rock.

It can be seen from the above formula that under the condition of no other factors affecting MFI, the magnetic susceptibility of rock samples is positively correlated with the stress.

On the other hand, the concrete failure process is the process of crack generation, expansion and penetration of the specimen under load. During this process, the sand particles and impurities inside the concrete will slip and dislocate [26], and these behaviors cause charges to accumulate, thereby forming opposite charges on the structural surface (as shown in Figure 15). During the failure process of concrete under load, the form of sliding, the magnitude of friction force, the degree of sliding and the speed have an impact on the magnetic field signal [27]. The change of the magnetic field signal reflects the development of internal cracks in the concrete to a certain extent. Triantis et al. [6,28] found the emission of electrical signals during application of mechanical stress to brittle geo-materials, originating as a result of the opening of cracks and microfractures in rock. This coincides with our research results.

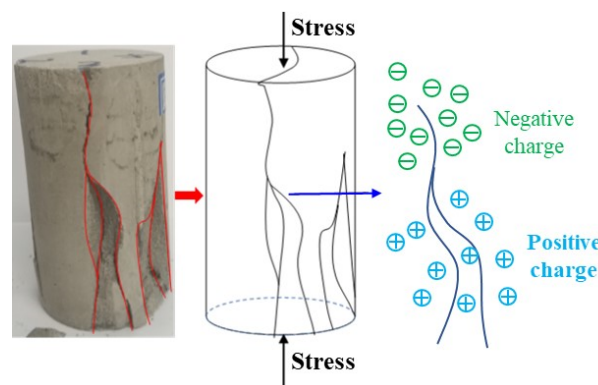


Figure 15. Schematic diagram of friction effect in concrete failure process.

Therefore, the magnetic field response mechanism during concrete loading failure should include the piezomagnetic and friction effects. The piezomagnetic effect is mainly related to the external stress and the composition of the concrete material. The higher the stress, the more piezomagnetic material it contains, the more MFI increases, and this phenomenon is sustainable. The experimental results in Figures 6–8 all verify this. The friction effect mainly occurs during the crack propagation process, and its effect is related to the material and heterogeneity of the concrete sample. The better the frictional electrification effect between the internal micro-particles, the stronger the instantaneous magnetic field generated.

7.3. Application of Magnetic Field Monitoring Technology in Industrial Production

Coal and rock dynamic disaster is a process in which coal and rock are destroyed under stress and lead to disaster. Affected by the complexity of geological conditions, the heterogeneity of coal and rock structure and the disturbance of mining engineering, the occurrence mechanism of coal and rock dynamic disasters is not clear, and its early warning accuracy needs to be improved. In this work, by magnetic field monitoring experiment of concrete, the feasibility of magnetic field monitoring the loading failure process of brittle materials was verified.

During the dynamic activity of coal and rock, the stress changes. The mining process of coal is a kind of unloading behavior. The mining or excavation area loses its bearing capacity, and the load will be transferred to other positions. As a result, pressure relief and crushing area, stress concentration area and original rock stress area are formed in front of the mining face or driving face. Among them, the pressure relief and crushing area and the stress concentration area are unstable areas, which are the main locations of coal–rock dynamic disasters. The accurate monitoring of the stress state and failure process of coal and rock mass can provide technical support for preventing and controlling mine dynamic disasters. The experimental results of the change law of the magnetic field in the concrete loading and failure process in this paper show that the loading and failure process of brittle materials will increase MFI around the material. Based on this principle, mine dynamic disasters can be monitored and early warning can be given.

In fact, the monitoring and early warning of coal rock electromagnetic radiation technology, AE technology and micro-seismic technology that have been applied now are mainly based on the stress state and fracture process of coal rock mass. This shows that the technology has the potential of application of coal and rock dynamic disaster monitoring and early warning technology. It is worth noting that the results in Figure 9 and the results of a large number of previous studies show that the AE iso-wave signal is often sudden, which is not conducive to the stable test and quantitative interpretation of coal and rock mass damage, which is the advantage of magnetic field monitoring technology.

8. Conclusions

In this paper, uniaxial compression, graded loading and cyclic loading experiments were carried out on concrete samples, the crack morphology and the change characteristics of the magnetic field in the concrete failure process under load were analyzed and the magnetic field change mechanism in the concrete failure process was revealed. The field application scenarios of magnetic field monitoring technology were proposed. The conclusions are as follows:

- (1) A magnetic field signal would be generated during the loading failure process of the concrete sample, which was accompanied by the whole loading process; the change of MFI during the loading process was in good agreement with the loading failure process of the concrete sample; in the uniaxial compression process, MFI showed a steady increase trend, but it would increase rapidly when the load-drop occurs in the sample.
- (2) Concrete showed obvious brittleness in the loading process, and there were many local fractures; local damage would cause fluctuations of MFI, but its effect was greatly affected by the rupture strength. The stronger the rupture, the more significant the change of MFI. The amount of change in MFI was not linearly proportional to the amount of change in load drop.
- (3) During the grading loading and cyclic loading and unloading of concrete, the value of MFI around the concrete sample was positively correlated with the load. When the concrete was in the constant load stage, MFI around the concrete remained basically stable; when the main rupture of the concrete sample occurred, the value of MFI reached a peak value, it did not keep at a high level all the time, but decreased rapidly.
- (4) There were two mechanisms for the generation of the magnetic field in the process of concrete failure under load, namely the piezomagnetic effect and the friction effect, which corresponded to the action of the load and the excitation of the fracture, respectively. The former caused the stable increase of MFI, and the effect was related to the influence of the content of the piezoelectric magnetic material in the material composition; the latter led to a sudden increase in the value of MFI, and the effect was related to the triboelectric effect of the micro-particles of the material.

This research reveals the change law of MFI and the generation mechanism of the magnetic field signal in the process of concrete failure under load. The research results are con-

ducive to the accurate prediction of the concrete magnetic field monitoring, and help to promote the development of mine dynamic disaster monitoring and early warning technology.

Author Contributions: Conceptualization, L.Q. and D.S.; software, S.Y.; validation, M.W.; formal analysis, J.L. and Y.T.; investigation, L.Q.; resources, D.S.; data curation, Y.T. and J.L.; writing—original draft preparation, L.Q.; writing—review and editing, L.Q.; supervision, D.S.; funding acquisition, L.Q. and D.S. All authors have read and agreed to the published version of the manuscript.

Funding: This research was funded by the National Natural Science Foundation of China (Grant No. 52004016, 52174162), the State Key Laboratory Cultivation Base for Gas Geology and Gas Control (Henan Polytechnic University) (Grant No. WS2020B01), the Planning Textbook Project of USTB (Grant No. JC2021JY007), the Science and Technology Support Plan Project of Guizhou Province ([2021]515).

Conflicts of Interest: The authors declare no competing financial interest or personal relationships that could have appeared to influence the work in this paper.

References

- Li, X.; Cao, Z.; Xu, Y. Characteristics and trends of coal mine safety development. *Energy Sources Part A Recovery Util. Environ. Eff.* **2020**, *2020*, 1–14. [[CrossRef](#)]
- Li, X.; Chen, S.; Li, Z.; Wang, E. Rockburst mechanism in coal rock with structural surface and the microseismic (MS) and electromagnetic radiation (EMR) response. *Eng. Fail. Anal.* **2021**, *124*, 105396. [[CrossRef](#)]
- Qiu, L.; Liu, Z.; Wang, E.; He, X.; Feng, J.; Li, B. Early-warning of rock burst in coal mine by low-frequency electromagnetic radiation. *Eng. Geol.* **2020**, *279*, 105755. [[CrossRef](#)]
- Guinea, G.; Sayed, K.; Rocco, C.; Elices, M.; Planas, J. The effect of the bond between the matrix and the aggregates on the cracking mechanism and fracture parameters of concrete. *Cem. Concr. Res.* **2002**, *32*, 1961–1970. [[CrossRef](#)]
- Lee, K.; Park, J. A numerical model for elastic modulus of concrete considering interfacial transition zone. *Cem. Concr. Res.* **2007**, *38*, 396–402. [[CrossRef](#)]
- Kyriazopoulos, A.; Anastasiadis, C.; Triantis, D.; Brown, C. Non-destructive evaluation of cement-based materials from pressure-stimulated electrical emission—Preliminary results. *Constr. Build. Mater.* **2011**, *25*, 1980–1990. [[CrossRef](#)]
- Li, D.; Wang, E.; Kong, X.; Zhao, S.; Kong, Y.; Wang, X.; Wang, D.; Liu, Q. Mechanical properties and electromagnetic radiation characteristics of concrete specimens after exposed to elevated temperatures. *Constr. Build. Mater.* **2018**, *188*, 381–390.
- Chen, J.; Wang, Q. Concrete damage nonlinear detection based on embedded ultrasonic sensors. *J. Appl. Acoust.* **2018**, *37*, 482–487.
- Esmailkhanian, B.; Feys, D.; Khayat, K.; Yahia, A. New test method to evaluate dynamic stability of self-consolidating concrete. *ACI Mater. J.* **2014**, *111*, 299–307. [[CrossRef](#)]
- Zou, Y. Application of PEEP verification and optimization of supporting design. *Coal Sci. Technol. Mag.* **2017**, *4*, 111–115.
- Ji, H.; Zhang, T.; Cai, M.; Zhang, Z. Experimental study on acoustic emission dynamic detection of concrete material damage. *Chin. J. Rock Mech. Eng.* **2000**, *19*, 165.
- Wu, S.; Zhang, S.; Shen, D. An experimental study on Kaiser effect of acoustic emission in concrete under uniaxial tension loading. *China Civ. Eng. J.* **2008**, *41*, 31–39.
- Wang, X.; Wang, E.; Liu, X.; Jia, H.; Li, D.; Wang, H. Time-frequency-space response of damage evolution for concrete based on AE-UT joint monitoring under step-loading. *J. China Univ. Min. Technol.* **2019**, *48*, 268–277.
- Zhang, H.; Sun, Q.; Ge, Z. Analysis of the characteristics of magnetic properties change in the rock failure process. *Acta Geophys.* **2020**, *68*, 289–302. [[CrossRef](#)]
- Zhang, F. Study on fracture evolution characteristics of concrete containing aggregate and its statistical damage constitutive model based on acoustic emission characteristics. *J. Water Resour. Water Eng.* **2020**, *31*, 182–188.
- Triantis, D.; Pasiou, E.; Stavarakas, I.; Kourkoulis, S. Hidden Affinities between Electric and Acoustic Activities in Brittle Materials at Near-Fracture Load Levels. *Rock Mech. Rock Eng.* **2022**, *55*, 1325–1342. [[CrossRef](#)]
- Chen, G.Y.; Xia, D.; Yu, Y.; Mao, C. Experimental study on stress-strain-magnetic intensity effect during rock compression. *J. Exp. Mech.* **2012**, *27*, 669–676.
- Zhang, G.; Zhang, J.; Jin, W.; Chen, J. Review of the Mechanics and Fatigue Researches on Magnetic Materials Based on Piezomagnetic Effect. *Mater. Rev.* **2014**, *28*, 4–10.
- Sharma, S.; Chauhan, V.; Sinapius, M. A review on deformation-induced electromagnetic radiation detection: History and current status of the technique. *J. Mater. Sci.* **2021**, *56*, 4500–4551. [[CrossRef](#)]
- Qiu, L.; Zhu, Y.; Song, D.; He, X.; Wang, W.; Liu, Y.; Xiao, Y.; Wei, M.; Yin, S.; Liu, Q. Study on the Nonlinear Characteristics of EMR and AE during Coal Splitting Tests. *Minerals* **2022**, *12*, 108. [[CrossRef](#)]
- Li, J.; Yan, X.; Ren, X. Large-sample experimental study on uniaxial compressive behavior of concrete under different loading rates. *J. Build. Struct.* **2016**, *37*, 66–75.
- Yin, S.; Song, D.; He, X.; Qiu, L.; Liu, Y. Experimental study on the change of magnetic field in the process of concrete failure under load. *Struct. Control Health Monit.* **2021**, *28*, e2806. [[CrossRef](#)]

23. Jin, L.; Du, X. Meso-scale numerical analysis of the effect of loading rate on the tensile failure behavior of concrete. *Eng. Mech.* **2015**, *32*, 42–49.
24. Qiu, L.; Song, D.; He, X.; Wang, E.; Li, Z.; Yin, S.; Wei, M.; Liu, Y. Multifractal of electromagnetic waveform and spectrum about coal rock samples subjected to uniaxial compression. *Fractals* **2020**, *28*, 2050061. [[CrossRef](#)]
25. Nagata, T. Application of tectonomagnetism to earthquake phenomena. *Tectonophysics* **1972**, *14*, 263–271. [[CrossRef](#)]
26. Sun, M. Experimental study and finite element analysis on the bond stress slip. *Rev. IBRACON Estrut. Mater.* **2015**, *8*, 787–799.
27. Fu, S. *Study on Characteristics and Generation Mechanism of Low-Frequency Magnetic Signals in Coal Failure under Static Load*; China University of Mining and Technology: Beijing, China, 2018.
28. Triantis, D.; Vallianatos, F.; Stavrakas, I.; Hloupis, G. Relaxation phenomena of electrical signal emissions from rock following application of abrupt mechanical stress. *Ann. Geophys.* **2012**, *55*, 207–212. [[CrossRef](#)]